Article | Received 23 June 2025; Revised 6 October 2025; Accepted 17 November 2025; Published 28 November 2025
https://doi.org/10.55092/mt20250005

Design of a generic hybrid mechanism for hydraulic actuation in humanoid shoulder joints

Wael Soukarieh[1], Maya Sleiman[1,2,*], Ahmad Tayba[3], Hang Su[1,*] and Samer AlFayad[1]

[1] IBISC Laboratory, University of Paris Saclay, 91034 Évry, France

[2] KALYSTA Actuation, 91000 Évry, France

[3] Independent researcher

* Correspondence author; E-mail: maya.sleiman@kalysta.tech (M.S.); hang.su@univ-evry.fr (H.S.).

Highlights:

- Introduces a novel hybrid serial-parallel shoulder mechanism for the HYDROïD humanoid robot, designed to be compact, powerful, and dexterous.
- Presents the complete Direct Geometric Model (DGM) for the proposed 4-DOF hybrid shoulder, enabling detailed kinematic analysis and performance validation.
- The proposed shoulder design achieves a Workspace Analysis Similarity for Robotic Arms (WAS_{RA}) of 26.13%, demonstrating high human-like motion with only shoulder actuation compared to other full-arm systems.
- The design successfully integrates a link-driven, four-bar-based mechanism with linear actuators to optimize the balance between a wide range of motion and high torque output in a compact volume.
- Demonstrates an efficient approach to humanoid joint design that enhances performance and adaptability, paving the way for simpler and more effective systems for human-robot interaction.

Abstract: This paper introduces a hybrid serial-parallel mechanism developed for the arms of the HYDROïD humanoid robot, aiming to enhance workspace while improving structural stiffness and rigidity. The mechanism is composed of two integrated substructures: a serial chain and a fully parallel subsystem. Although hybrid architectures have been underexplored in humanoid robotics, their combination of serial and parallel advantages presents a promising solution to challenges such as compactness and the varied range of motion required in pitch, yaw, and roll directions. A key design objective is to maintain a slim and anthropomorphic form to facilitate effective and intuitive human-robot interaction. To meet this criterion, the modified Hanavan model was used to determine the geometric and inertial properties of the robot's upper body, particularly the shoulder mechanism. For initial spatial approximation, the shoulder joint and upper torso were modeled using simplified geometries such as cylindrical cones or bounding parallelepipeds to respect the compact design envelope. These spatial constraints support the use of hybrid architectures over purely parallel configurations. Finally, the kinematic performance of the proposed mechanism is validated through numerical simulations of the workspace and joint torques, demonstrating

the feasibility and effectiveness of the hybrid design approach in humanoid robotics.

Keywords: humanoid robot; shoulder mechanism; hybrid mechanism; kinematic analysis; workspace analysis; hydraulic actuation; hybrid serial-parallel; kinematic structure

1. Introduction

In recent years, rapid advances in technology have fostered the development of humanoid robots designed for seamless human interaction through cutting-edge mechatronic innovations. These robots, which differ in form, scale, and functionality, are built to replicate human behaviors, appearances, and tasks. Their utility spans hazardous environments and collaborative industrial settings, where they enhance efficiency, safety, and performance by extending human capabilities as shown in Figure 1. A significant design challenge lies in developing robotic arms that are strong, compact, and agile, enabling performance comparable to or better than that of humans.

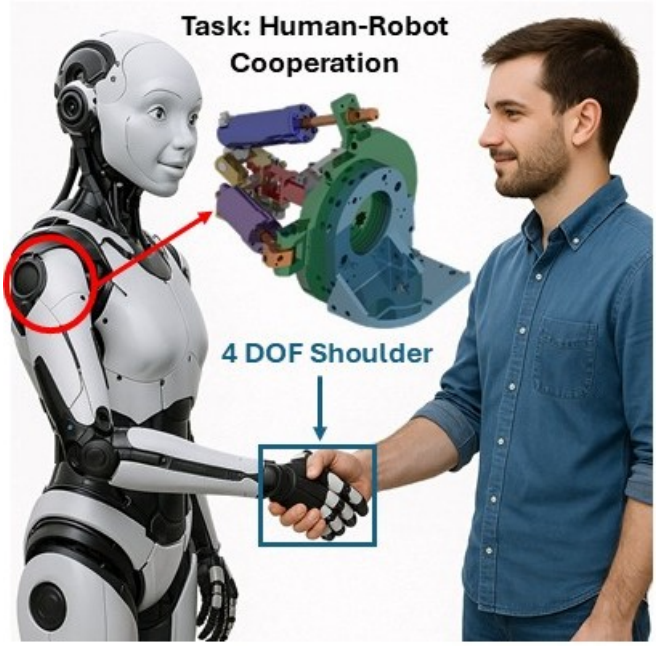

Figure 1. Highlighting the importance of 4 DOF shoulder mechanism in enhancing human-robot interaction.

Humanoid robotics is an interdisciplinary domain, drawing on biomechanics, medical data, engineering, and advanced modeling. It has witnessed substantial progress in areas such as locomotion, control, communication, and mechatronic systems. With the recent surge in full-scale humanoid development, three main families have emerged (see Table 1).

The Atlas family [1], which features hydraulically powered robots like PETMAN capable of agile, high-performance tasks in rough environments. The HRP-5P series [2], electro-mechanically actuated robots include ASIMO [3] and Figure-01 [4], designed for daily human-interactive tasks with greater degrees of freedom. The Optimus Gen II group [5], which includes electric humanoids such as TALOS [6] and the Unitree H1-2 [7], a humanoid robot designed for both mobility and perception-rich interaction tasks.

Table 1. Specifications of three humanoid robots: Atlas, HRP-5P, and Optimus Gen-II.

Atlas [1]	HRP-5P [2]	Optimus [5]
2016	2018	2023
28	37	28
80 Kg	101 Kg	63 Kg
Hydraulic/Electric	Electric	Electric
Heavy-duty tasks	Human mimicry and real-world applications	Interaction and human resemblance

Humanoid robots in the early stages focused on replicating human gait and locomotion, with research mainly directed at lower-body movement [8]. However, more comprehensive capability requires complex interaction with the environment, which shifts focus to upper-body manipulation. This transition underscores the growing importance of sophisticated, dexterous arm designs, specially the shoulder mechanism which is instrumental in achieving human-like movement and control [9].

A number of robotic shoulder mechanisms have been described in literature, each being another trade-off between compactness, range, and torque output. The most common solution is the serial ball-and-socket configuration powered by three orthogonal rotary motors, offering a big workspace but poor load capacity due to cantilevered forces. Classic examples are the shoulders of the iCub [10] and the DLR Light-Weight Robot (LWR) series [11]. Parallel shoulder mechanisms on the other hand distribute loads across multiple closed-loop linkages, achieving higher stiffness and payload capability. However, they are rarely utilized as an exclusive solution in general-purpose humanoid robots due to their typically restricted workspace and dexterity and are instead frequently applied in rehabilitation exoskeletons and industrial manipulators with special tasks. Hybrid solutions have also been investigated, such as the Pandora robot shoulder, which combines serial and parallel architectures to compromise workspace and stiffness [12]. More recent solutions incorporate translational DOFs at the shoulder girdle, such as HRP-5P, to mimic clavicle and scapula motion for greater anthropomorphism [2]. These different methods show that while many solutions have been put forward, a compact, efficient, and human-like shoulder remains an active challenge in humanoid robotics.

To meet the demanding specifications of human-robot interaction, a humanoid shoulder must be (i) compact, (ii) light, (iii) highly dexterous, and (iv) inherently safe. Compactness facilitates maneuverability in restricted spaces and reduces the risks of collision. Light structures provide increased speeds of movement and energy efficiency [13,14]. Dexterity-achieved through articulated mechanisms and multifunctional end-effectors-is critical for effective interaction [15].

These systems are designed following large volumes of information on human motion, which guides the creation of polymorphic mechanisms that imitate the human form. Mechanically, robots are either serial or parallel. Serial manipulators, being composed of joints in series, provide large workspaces and high dexterity and are therefore adequate for fine manipulation but often limited in load [16]. Parallel mechanisms, with multiple links joining the base to an end-effector in closed loops, offer enhanced rigidity and payload capability at the cost of a reduced range of motion [17].

To exploit the strengths and mitigate the weaknesses of both types, hybrid mechanisms emerge [18].

These incorporate parallel mechanisms at the base-for strength and stability-with serial chains at the distal end for long motion and flexibility. This synergy enables more human-like function, combining precision and robustness.

The shoulder mechanism is critical in achieving human-like dexterity [19]. It determines the robot's ability to carry out both simple and complex tasks, requiring large motion range and dynamic diversity [20]. Table 2 shows the range of motion and joint volume of the human shoulder [21], indicating the significance of abduction, flexion, and rotation in having large task coverage.

Table 2. Shoulder articulation range of motion on the 3 DOFs and volume.

Articulation	Movement	Range of Motion [Degrees]	Volume (ml) [22]
3*Shoulder [21]	Extension–Flexion	(50–180)	
	Abduction–Adduction	(180–30)	1848.2
	Internal–External Rotation	(100–80)	

Selecting the appropriate kinematic structure is fundamental for achieving bi-manual manipulation and natural interaction [23]. The shoulder design must enable the end-effector to reach all necessary workspace points comfortably [24]. Despite numerous mechanism choices, optimizing for human-like performance remains a key objective [25]. Different families employ varying shoulder solutions. Atlas, for instance, integrates a ball-and-socket joint actuated by three rotary actuators. HRP-5P enhances this with two additional linear actuators for translational shoulder motion. These examples highlight that hybrid configurations combining serial and parallel elements offer promising paths to more natural movement.

This study introduces a novel shoulder mechanism design for the humanoid robot HYDROïD—a full-scale robot under development with 36 hydraulic joints. As shown in Figure 2, HYDROïD's arm mechanism is engineered to optimize torque output, mechanical volume, and motion range [26]. The remainder of this paper is structured as follows: Section 2 details the hybrid mechanical concept; Section 3 explores the kinematic configuration; Section 4 presents the simulation and evaluation; and Section 5 concludes with insights and directions for future research.

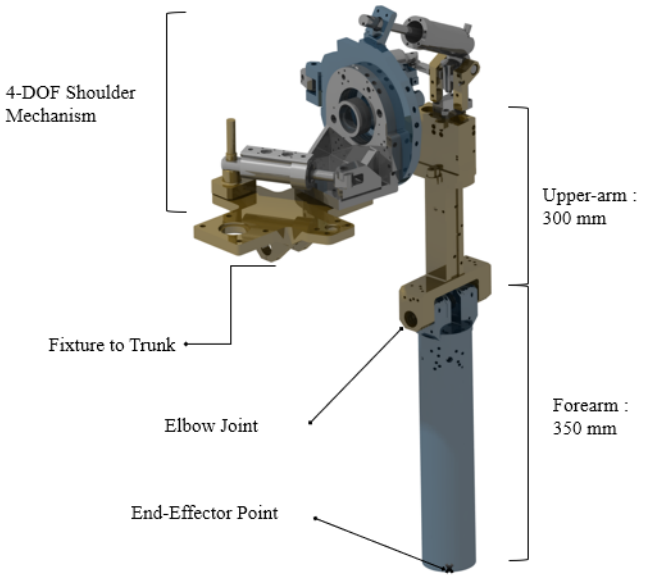

Figure 2. HYDROïD's shoulder, a long cylinder is installed to replicate the forearm.

2. Proposed hybrid structure

Building on the limitations identified in existing designs, the HYDROïD project introduces a novel hybrid shoulder mechanism that integrates the advantages of both serial and parallel architectures. While serial joints provide a wide and dexterous workspace, they suffer from limited load-bearing capacity due to cantilevered structures. Conversely, parallel mechanisms offer high stiffness and torque transmission but are restricted in workspace coverage. By combining these two principles, the proposed hybrid design achieves a balance between range of motion, strength, and compactness, directly addressing the shortcomings of conventional approaches.

The mechanism's kinematic structure is developed under biomechanical constraints derived from the Modified Hanavan Model [22], which defines the allowable spatial envelope of the human shoulder in terms of volume and motion limits. This ensures that the resulting design not only meets mechanical efficiency criteria but also preserves anthropomorphic fidelity, enabling natural and safe human-robot interaction.

The developed configuration synthesizes serial and parallel sub-mechanisms to generate diverse motions across the three principal degrees of freedom, while also optimizing torque output and structural stability. This enables HYDROïD to replicate natural shoulder dynamics more accurately than traditional designs, offering an efficient, versatile, and human-like solution for advanced humanoid robotics applications.

3. Shoulder drive mechanism

The choice of a drive mechanism critically influences both the power transmission efficiency and the overall weight of a humanoid robot's upper limb. Each drive type presents distinct advantages and limitations, making the choice a critical design decision. In humanoid robotics, drive mechanisms generally fall into three main categories: tendon-based, gear-based, and link-based systems [27].

- Tendon Drives use cables and pulleys to transfer force and actuate joints. They offer lightweight construction, flexibility, and allow for remote actuation. However, these systems can be mechanically intricate, requiring careful routing to minimize friction, wear, and mechanical losses [28].
- Gear Drives transmit motion and torque through interlocking gears, providing stiffness, and effective power delivery across a range of loads. Their main drawback is that gears tend to be bulkier and heavier compared to other drive options, which can increase the limb's overall mass [29].
- Linkage Drives are mechanical linkages to connect segments, enabling specific joint behaviors and coordinated motion. A common example is the four-bar linkage, which generates parallel motion depending on the configuration. The dimensions of the links play a crucial role in defining the system's reachable workspace [30].

Considering the design requirements for a compact and rigid humanoid mechanism, traditional gear or tendon drives are not optimal. Gear drives are often heavy and bulky, making them not suitable when designing an anthropomorphic mechanism. Tendon drives offer a lightweight solution but can be complex to route and lack the stiffness required for high force interactions in duties required by HYDROïD. To address these limitations, we adopted linear hydraulic actuators that offer a high power-to-weight ratio

allowing the mechanism to generate sufficient force and torque output within minimal volume.

The link drive mechanism is suitable for our design goals, because it allows for the creation of a scalable hybrid mechanism. The link drive utilized in the development of this mechanism is based on a double rod-crank system. Traditionally, a single rod-crank system (Figure 3a) transforms reciprocating motion into rotation but can encounter singular positions (Figure 3b). To solve this, a two-crank mechanism is used (Figure 3c). When one mechanism is in a singular position, the other can provide the necessary rotation to unlock it (Figure 3d). Our proposed solution hence uses two linear actuators to drive this double rod system (Figure 3e), generating a large range of motion. The shoulder mechanism therefore has 3-DOF, composed of 17 joints in three kinematic chains, forming two independent closed loops. An additional fourth degree of freedom for shoulder protraction/retraction allows the arm to extend or retract, improving the robot's interaction with its environment.

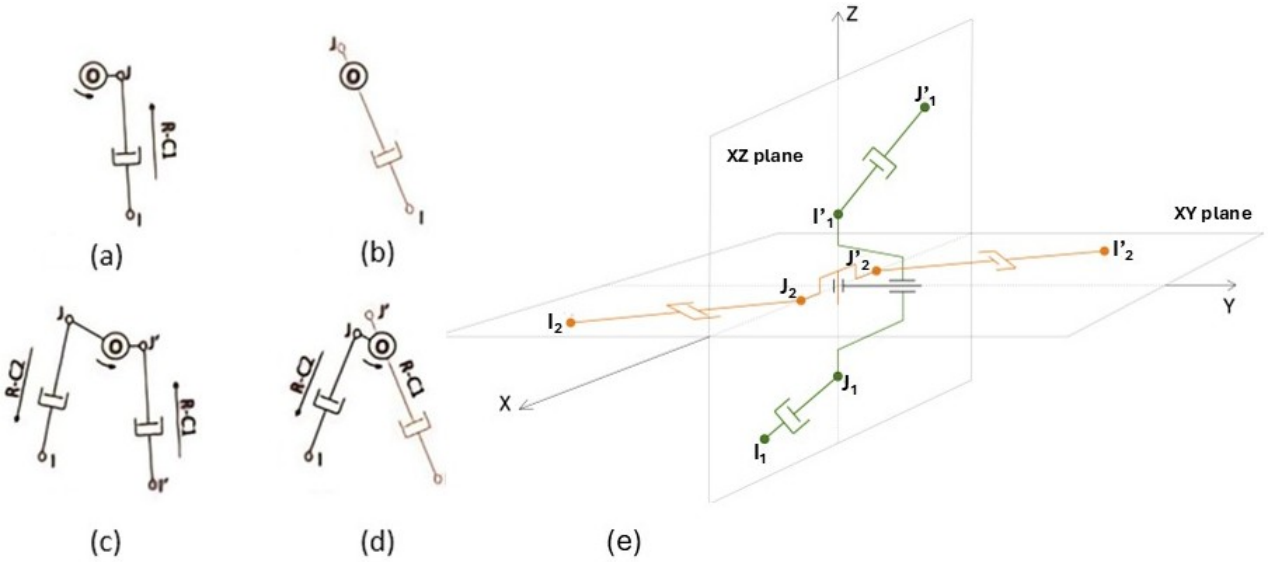

Figure 3. Rod-Crank systems [31]: **(a)** Rod-crank mechanism; **(b)** Singularity in a rod-crank mechanism; **(c)** Double rod-crank mechanism; **(d)** Unlocked singularity in a rod-crank mechanism; **(e)** Proposed shoulder design: Rod-Crank system with 2 outputs.

3.1. Kinematic description

The developed shoulder requires generating two perpendicular rotations at the output. The four rod-crank systems have the potential to generate these rotations. As shown in Figure 4, the arrangement of two rod-crank systems $[I_1J_1]$ & $[I_1^{'}J_1^{'}]$ in the XZ plane, rotating around the Y axis is guaranteed, while the other two rod-crank systems $[I_2J_2]$ & $[I_2^{'}J_2^{'}]$ in the XY plane provide rotation around the Z axis.

While every one of the above tendon, gear, and linkage drives has its own set of benefits, conventional ways of creating these two orthogonal rotations have a tendency to create large and inefficient mechanisms. Compared to strictly serial or parallel designs, our approach is a fundamentally novel and generic hybrid mechanism that combines the best of both to counterbalance their limitations. The primary innovation lies in its spatially efficient 3D configuration that does the same amount of work with just two linear hydraulic actuators for four different rod-crank systems. The hydraulic actuators also are capable of providing the required efforts for actuating this mechanism as intended. This innovative combination

is a significant deviation from current designs such as that of AlFayad *et al.* [32], who conducted other kinematic configurations. As can be seen from Figure 4, the linear actuators, [DF] & [EG], are arranged such that their projections equal the four actuators needed to make the four rod-crank mechanisms and by that also avoiding singular position. The novel kinematic layout not only overcomes the size constraint of the HYDROïD robot but also provides a generic model for compact, high-strength joint design applicable to a wide range of humanoid robotics.

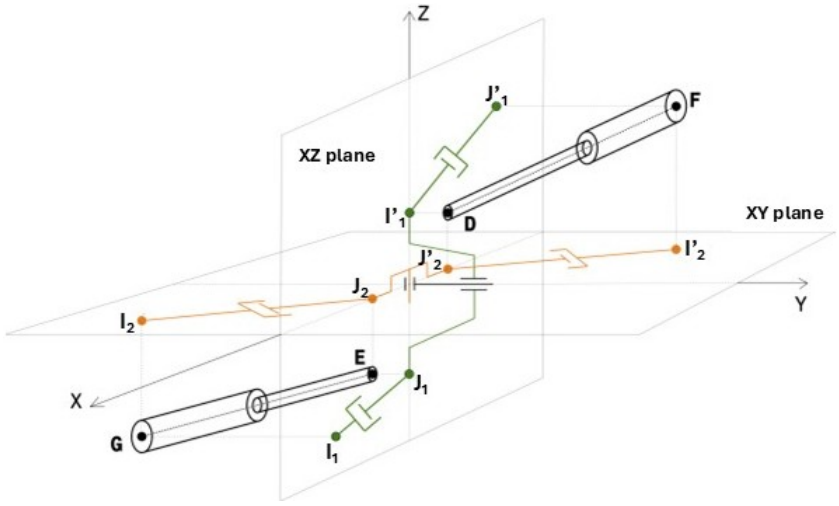

Figure 4. Proposed solution. Two linear actuators produce the rotations at the output. Pistons in the XY and XZ planes are the projections of the linear actuators.

Designing a hybrid mechanism presents two main challenges: (i) determining the appropriate kinematic structure and the sequence of serial and parallel chains, and (ii) proposing and optimizing the mechanism itself. To tackle the first challenge, various studies have investigated the sequencing of chains in hybrid designs. For instance, AlFayad *et al.* [32] proposed a configuration where the pitch motion is handled by a serial chain at the front end. This choice plays a critical role in minimizing the overall size of the mechanism, as it allows the parallel section to be more compact. This strategy illustrates the inherent trade-off between maximizing the range of motion and maintaining a compact design.

In the context of link-driven systems-especially the four-bar rod-crank configuration-this methodology shows strong potential for achieving extensive motion within a constrained space. By strategically integrating linear actuators and refining the kinematic layout, the resulting hybrid mechanism can deliver both high performance and efficiency in replicating complex shoulder movements.

3.2. Parameter description

After exploiting the various approaches and then reaching to the four rod-crank system, the proposed shoulder mechanism is introduced in Figure 5. Each limb and joint axis of the fully parallel chains are respectively denoted as ${}^{j}C_i$ and $\mathbf{Z}^i_j$, where $j = 1,2$ indicates the kinematic chain index the frame belongs to, and $1 \leq i \leq 9$ as shown in Figure 5, where $(A,B,D,E,F,\&\ G)$ represent the centers of the links $(C^1_3, C^2_3, C^1_4, C^2_4, C^1_6, \&\ C^2_6)$ respectively. The relative coordinates for these centers concerning the previous link are defined as $A(X^f_A, Y^f_A, Z^f_A)$, $B(X^f_B, Y^f_B, Z^f_B)$, $D(X^{3,1}_D, 0, Z^{3,1}_D)$, $E(X^{3,2}_E, 0, Z^{3,2}_E)$, $F(X^0_F, Y^0_F, Z^0_F)$, and $G(X^0_G, Y^0_G, Z^0_G)$ respectively.

Parameter values (in mm):

$X_A^f = 158.01$	$X_D^{3,1} = 29.23$	$X_F^0 = 114.65$	$X_B^f = 133.138$
$X_E^{3,2} = 32.70$	$X_G^0 = 129.51$	$-Y_A^f = 30$	$-Y_F^0 = 0$
$-Y_B^f = 30$	$Y_G^0 = 129$	$R_1 = 50.83^{+45}_{-}$	$R_2 = 28.41^{+25}_{-}$

Due to the generic configuration of the proposed hybrid mechanism, certain parameters must be assigned explicit values to fully specify the design (see Figure 5 for parameter definitions). The chosen parameter values are detailed in the Denavit-Hartenberg Table 3. Once the new kinematic structure is established, a performance analysis is required. This analysis will be based on the detailed geometric models presented in the following section.

This section presents the modeling and kinematic evaluation of the proposed robotic arm mechanism, with emphasis on two essential components: the Direct Geometric Model (DGM) and its numerical validation through simulation. The goal is to assess the mechanism's spatial reach and functional performance, ensuring alignment with the intended operational specifications.

Table 3. Modified DH parameters of the hybrid mechanism.

j	i	σ_j	γ_j	b_j	α_j	d_j	θ_j	r_j
C_v	C_0	0	0	0	0	0	θ_v	0
C_f	C_v	0	0	0	$\frac{\pi}{2}$	0	$-\theta_f - \frac{\pi}{2}$	0
C_3^1	C_f	0	0	0	$\frac{\pi}{2}$	X_A^f	$\theta_3^1 - \theta_3^{1,0}$	$-Y_A^f$
C_4^1	C_3^1	0	0	0	$\frac{\pi}{2}$	$X_D^{3,1}$	$\theta_4^1 + \theta_4^{1,0}$	0
C_5^1	C_4^1	0	0	0	$\frac{\pi}{2}$	0	θ_5^1	0
$R_C^{1,\text{left}}$	C_5^1	0	0	0	0	0	0	0
C_6^1	C_0	0	0	0	0	X_F^0	$\theta_6^1 + \pi$	$-Y_F^0$
C_7^1	C_6^1	0	0	0	$\frac{\pi}{2}$	0	$\theta_7^1 + \frac{\pi}{2}$	0
C_8^1	C_7^1	0	0	0	$\frac{\pi}{2}$	0	$\theta_8^1 - \theta_8^{1,0}$	0
C_9^1	C_8^1	1	0	0	α_9^1	0	0	$-R_1$
$R_C^{1,\text{right}}$	C_9^1	0	0	0	0	0	$-\frac{\pi}{2}$	0
C_3^2	C_f	0	$-\frac{\pi}{2}$	0	$\frac{\pi}{2}$	X_B^f	$\theta_3^2 - \theta_3^{2,0}$	$-Y_B^f$
C_4^2	C_3^2	0	0	0	$\frac{\pi}{2}$	$X_E^{3,2}$	$\theta_4^2 + \theta_4^{2,0}$	0
C_5^2	C_4^2	0	0	0	$\frac{\pi}{2}$	0	θ_5^2	0
$R_C^{2,\text{left}}$	C_5^2	0	0	0	0	0	0	0
C_6^2	C_0	0	0	0	0	X_G^0	$\theta_6^2 + \pi$	$-Y_G^0$
C_7^2	C_6^2	0	0	0	$\frac{\pi}{2}$	0	$\theta_7^2 + \frac{\pi}{2}$	0
C_8^2	C_7^2	0	0	0	$\frac{\pi}{2}$	0	$\theta_8^2 + \theta_8^{2,0}$	0
C_9^2	C_8^2	1	0	0	$-\alpha_9^2$	0	0	$-R_2$
$R_C^{2,\text{right}}$	C_9^2	0	0	0	0	0	$-\theta_C^2$	0

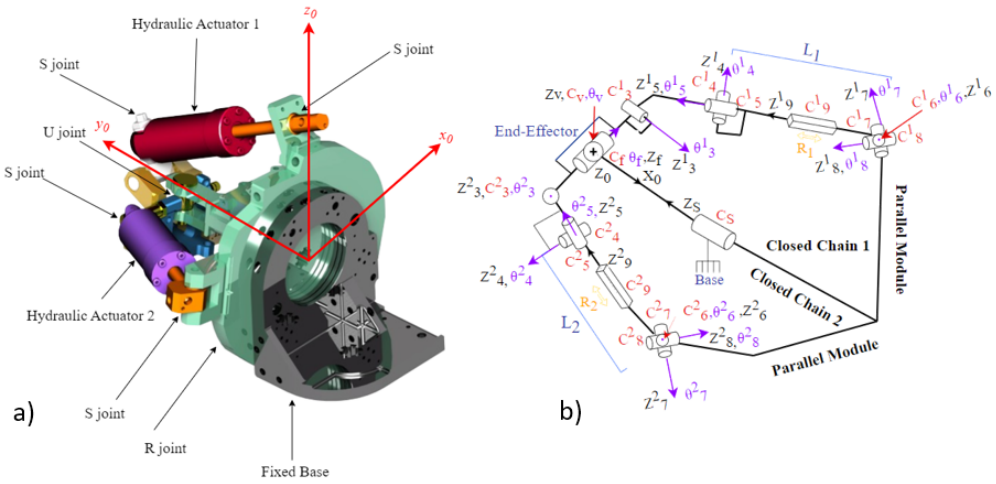

Figure 5. The novel generic hybrid mechanism. **(a)** CAD Render: Mechanism actuators demonstration; **(b)** The kinematic structure of the mechanism with DH parameters.

3.3. Direct Geometric Model (DGM)

The Direct Geometric Model (DGM) plays a central role in kinematic analysis and workspace evaluation. It enables the calculation of the end-effector's position and orientation based on known actuator lengths ($\mathscr{L}_j, j = 1,2$) and joint angles. In contrast to the Inverse Geometric Model (IGM), which computes actuator configurations for a given posture, the DGM derives the spatial coordinates of the end-effector from the actuator inputs.

The DGM is essential for several reasons. First, it facilitates the exploration and mapping of the arm's reachable workspace by systematically varying actuator lengths within their physical limits. This analysis ensures the mechanism can meet task-specific spatial requirements. Second, a precise formulation of the DGM is crucial for the accurate control of the arm during operation.

Using the Denavit-Hartenberg parameters provided in Table 3 and the kinematic structure illustrated in Figure 5, the transformation matrices for the mechanism are derived as follows:

Main branch transformation:

$$T_{\text{main}} = T_s \cdot T_v \cdot T_f \tag{1}$$

Closed chain 1 transformation:

$$T_{\text{closed chain 1}} = T_{13} \cdot T_{14} \cdot T_{15} \cdot T_{16} \cdot T_{17} \cdot T_{18} \cdot T_{19} \tag{2}$$

Closed chain 2 transformation:

$$T_{\text{closed chain 2}} = T_{23} \cdot T_{24} \cdot T_{25} \cdot T_{26} \cdot T_{27} \cdot T_{28} \cdot T_{29} \tag{3}$$

Where:

$$T = \begin{bmatrix} \cos(\theta) & -\sin(\theta)\cos(\alpha) & \sin(\theta)\sin(\alpha) & a\cos(\theta) \\ \sin(\theta) & \cos(\theta)\cos(\alpha) & -\cos(\theta)\sin(\alpha) & a\sin(\theta) \\ 0 & \sin(\alpha) & \cos(\alpha) & d \\ 0 & 0 & 0 & 1 \end{bmatrix} \tag{4}$$

The closed chains affect the transformation from the shoulder base C_s to the end effector C_f. Thus, studying the effect of the two closed chains will lead to a new transformation matrix T_{prime}. The branch

defined by $T_{\text{closed chain 1}}$ is multiplied by the inverse of the branch by $T_{\text{closed chain 2}}$ to take into consideration the effect of these branches on the main branch T_{main}.

Thus:

$$T_{\text{prime}} = T_{\text{closed chain 1}} \times T^{-1}_{\text{closed chain 2}} \tag{5}$$

Ultimately, the T_{total} matrix captures the complete transformation from the main branch (T_{main}) to the end-effector, accounting for the influence of both sub-branches ($T_{closed\,chain\,1}$ and $T_{closed\,chain\,2}$). Calculating T_{total} reveals how the combined kinematic contributions of the sub-branches affect the main structure. This matrix comprehensively reflects all positional and rotational changes throughout the closed-chain system, effectively characterizing the overall motion and configuration of the hybrid mechanism.

The total transformation is given by:

$$T_{\text{total}} = T_{\text{main}} \times T_{\text{prime}} \tag{6}$$

Thus, the full Direct Geometric Model (DGM) is given by the following transformation matrix:

$$T_{\text{total}} = f(\theta_v, \theta_f, \theta_{13}, \theta_{14}, \theta_{15}, \theta_{16}, \theta_{17}, \theta_{18}, \theta_{19}, \theta_{23}, \theta_{24}, \theta_{25}, \theta_{26}, \theta_{27}, \theta_{28}, \theta_{29}, L_1, L_2) \tag{7}$$

The Direct Geometric Model (DGM) serves as a fundamental tool for accurately characterizing and predicting the motion of the robotic arm. By capturing the complete kinematic chain, it enables precise modeling of the mechanism's response to actuation. This detailed representation is crucial not only for simulating motion behavior but also for facilitating further analyses. In particular, it establishes the basis for the workspace evaluation presented in the subsequent section, where the spatial reach and limitations of the mechanism are thoroughly examined.

4. Numerical validation

To test and evaluate the kinematic analysis presented in the previous section, numerical simulations were conducted. The Direct Geometric Model is the mathematical expression of our suggested mechanism's motion, using it we were able to perform a thorough investigation of the workspace and dynamic behavior of the mechanism, ensuring that the design of the mechanism is in accordance with the required functional outcomes.

Numerical simulations play a critical role in the design phases of robotic mechanisms, they offer insights on the mechanism characteristics before prototyping it. Using the DGM developed in Section 4, the first validation phase focused on testing the reachable workspace of the mechanism. The test was done to validate the arm's range of motion to guarantee that it can perform its intended functions effectively in a task space. Then second validation phase utilized multi-body dynamics programs to analyze the mechanical performance of the system is was conducted. The simulations aimed at exploring joint-space performance metrics such as workspace analysis, no-load joint torques, flexion/extension torque under a load, and recorded actuator speeds.

4.1. Workspace

The developed shoulder mechanism features four degrees of freedom (DOFs): abduction/adduction, flexion/extension, internal/external rotation, and protraction/retraction. This configuration offers a broader

range of motion than traditional designs [21], enabling the robotic arm to access more spatial positions. To evaluate biomechanical fidelity, the robot's workspace was overlaid with that of a human shoulder in a unified spatial map, allowing a visual comparison of reachability and motion similarity.

Workspace definition is challenging and typically addressed using three methods: iterative, deterministic, and analytical [24]. The Monte Carlo method, a common iterative approach, uses random joint sampling with forward kinematics to approximate the reachable workspace-suitable for high-DOF systems but computationally expensive [33].

Deterministic methods often rely on CAD and simulation tools to assess reach by executing defined joint trajectories, but they may overlook variability and uncertainties in real-world conditions [34]. Alternatively, analytical techniques-adopted in this work-use Denavit-Hartenberg (D-H) parameters to derive closed-form relations between joint angles and end-effector positions. This method offers high efficiency for systems with fewer DOFs, though its scalability is limited in more complex mechanisms [35].

To assess the mechanism's anatomical and functional fidelity, its performance is bench-marked against a 4-DOF human shoulder model. We quantify this comparison using the workspace anthropomorphic score (WAS_{RA}), a metric proposed by Sinha *et al* [36] and tested for various robots. The score offers a normalized measure of anthropomorphic performance by calculating the ratio between the robot arm's reachable volume, $Vol(W_{arm})$, and the union of both human and robot workspaces, $Vol(W_{Union})$.

$$WAS_{RA} = \frac{Vol(W_{arm})}{Vol(W_{Union})} \times 100\% \tag{8}$$

The WAS_{RA} score essentially measures how closely a robot's range of motion mirrors a human's, with a 100% score indicating a perfect overlap. Our analysis reveals that HYDROïD' shoulder, equipped with a 450 mm bar representing the length of a human arm connected to the mechanism, achieves a WAS_{RA} of 26.13%. What makes this result particularly impressive is its source: the shoulder joint alone. Table 4 puts this achievement into perspective by comparing it with several fully articulated robotic arms.

Table 4. Workspace Anthropomorphic Scores (WAS_{RA}) among humanoid robots.

Robot	Actuation Type	WAS_{RA} (%)
HYDROïD	Shoulder only	26.13
Atlas	Shoulder, Elbow, Wrist	17.41
iCub – IIT	Shoulder, Elbow, Wrist	37.54
NTU-IMI – NTU	Shoulder, Elbow, Wrist	42.81

The score of HYDROïD (26.13%) exceeds that of the entire arm of the Atlas robot (17.41%). This difference can be linked to the expected design goals of the two robots. While Atlas is engineered for high impact dynamic tasks like running and jumping, prioritizing durability, stiffness, and power, its design may focus less on the ranges of motion. On the other hand, HYDROïD's shoulder mechanism is specifically optimized for a high range of motion within a compact space, resulting in a more human-like reach for a single joint.

Although systems like iCub and NTU-IMI achieve higher scores based on actuating the shoulder, elbow, and wrist. This highlights the efficiency of the proposed shoulder-only mechanism that presents a

competitive workspace with minimal actuation. Figure 6 presents a comparison between HYDROïD and human shoulder workspaces, illustrating the motion range across the frontal, lateral, and coronal planes.

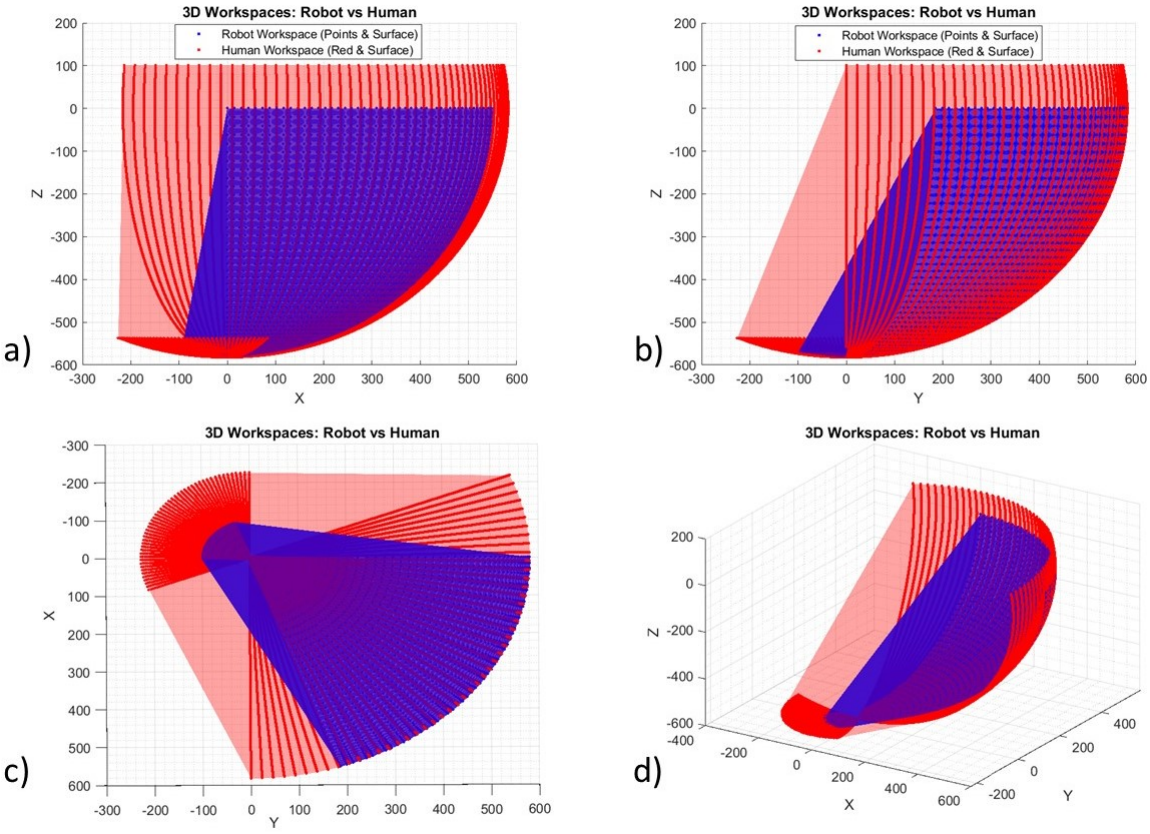

Figure 6. Robot *vs.* human workspace results; **(a)** The projection of the workspace on the ZX plane; **(b)** The projection of the workspace on the ZY plane; **(c)** The projection of the workspace on the XY plane; **(d)** An isometric view of the full 3D workspace.

4.2. Torque, force and speed analysis

The shoulder mechanism's dynamic behavior was evaluated under different motion scenarios, with particular emphasis on the torque requirements needed for smooth and reliable joint actuation. Several types of shoulder joint movements were studied, allowing for an in-depth assessment of the corresponding torque, force, and velocity profiles.

Movements such as flexion/extension, abduction/adduction, and internal/external rotation were modeled and simulated using ADAMS software. These simulations aimed to explore how each motion translates into mechanical demands at the joints. To gain a comprehensive view of the system's response, two conditions were considered: a load-free case and one involving an external load.

Following the simulations, the torque and speed outputs at the actuated joints were analyzed to capture the mechanism's real-time dynamic response. These parameters are critical in robotic arm design, as they directly influence both performance efficiency and operational safety. Through this detailed analysis, we aim to highlight how the HYDROïD shoulder contributes to the overall dynamics of the full robotic arm.

4.2.1. Motion 1: full rotation (flexion/extension)

The shoulder enables flexion and extension, allowing the arm to move in the sagittal plane. This test estimates the torque required for this motion under no-load conditions, within the natural range specified in Table 2. A harmonic function is used to generate a smooth periodic motion profile for simulating shoulder flexion/extension. The function is defined as:

$$\theta(t) = A \cdot \sin(\omega t + \phi) \tag{9}$$

Where $\theta(t)$ represents the angular displacement of the joint, A is the amplitude, defining the maximum angle of movement, ω is the angular frequency, and ϕ is the phase shift. The chosen function was used to simulate shoulder movement spanning 65 degrees to represent this motion within the ADAMS software and was divided into discrete increments of 5 degrees. The simulation results, presented in Figure 7, illustrate the corresponding torque and angular velocity profiles. The torque generated at the shoulder joint is determined using the following equation:

$$\tau_m = J^T F_g \tag{10}$$

Where τ_m is the joint torque, J is the Jacobian matrix for the system, and F_g represents the applied forces, including the gravitational load acting on the arm.

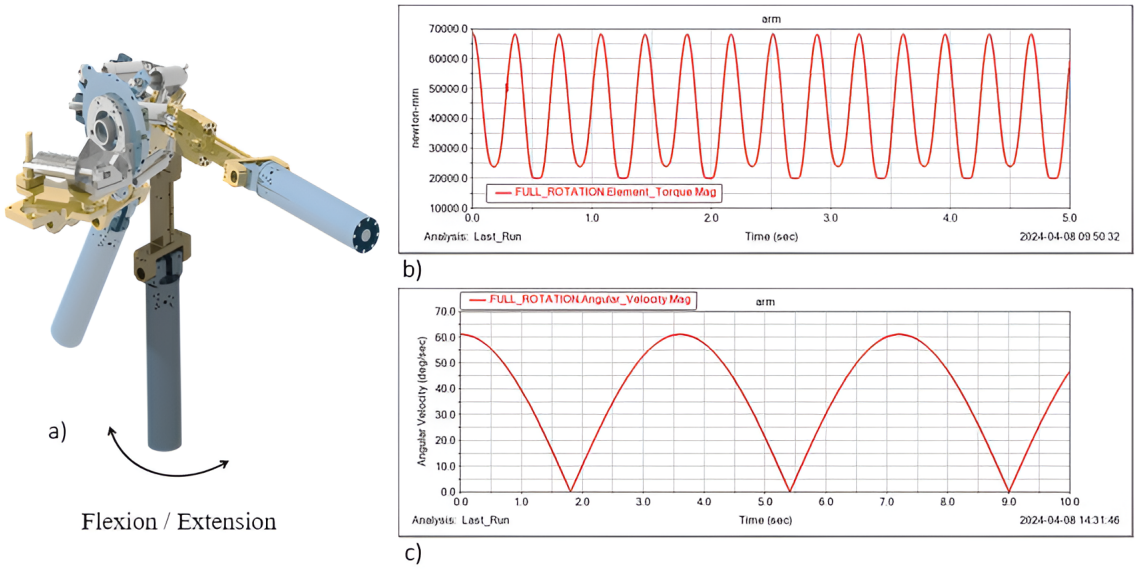

Figure 7. The figure shows the analysis of the shoulder's flexion/extension movement. **(a)** illustrates the motion of the robot arm in the sagittal plane; **(b)** presents the required joint torque under no-load conditions, with a peak torque of 68 N·m demonstrating the power needed for this movement; **(c)** shows the angular speed, a smooth sinusoidal curve as a result of the simple harmonic function used for simulation.

The motion was modeled in ADAMS software using a simple harmonic function defined as SHF(time, initial position, angular range, step size). For the shoulder flexion/extension, an average motion range of 65 degrees was simulated with increments of 5 degrees. This movement is fully characterized by the function SHF(time/0.1, 0.0, 65°, 5°), as specified in the referenced table. The resulting simulation, shown in Figure 7, yielded the required torque and angular velocity profiles.

4.2.2. Motions 2 and 3: abduction/adduction and internal/external rotations

Two hydraulic cylinders, labeled cylinder 1 and cylinder 2, generate abduction/adduction and internal/external rotation, respectively. Using the same approach, simple harmonic functions (SHF) in ADAMS software simulate these motions. Rod displacements of C_9^1 and C_9^2 as mentioned in Table 3 vary between the minimum and maximum positions defined in Table 2, following SHF(time, initial position, maximum displacement, step size). Specifically, SHF(time/2, 0.0, 50, 5) and SHF(time, 0.0, 30, 100) are used for motions 2 and 3. Simulation results in Figures 8 and 9 provide the required actuator forces and linear velocities.

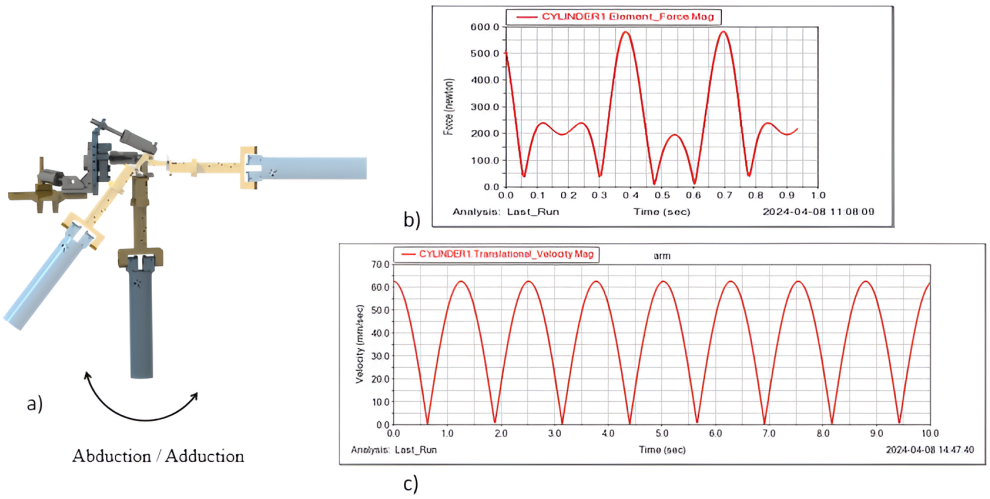

Figure 8. The figure displays the analysis of the shoulder's abduction/adduction movement. **(a)** illustrates the arm's motion as it moves away from and toward the body's midline; **(b)** shows the force required from the hydraulic cylinder, which reaches a peak of around 590 N to perform this movement; **(c)** presents the linear speed of the hydraulic actuator, confirming a smooth and consistent velocity profile.

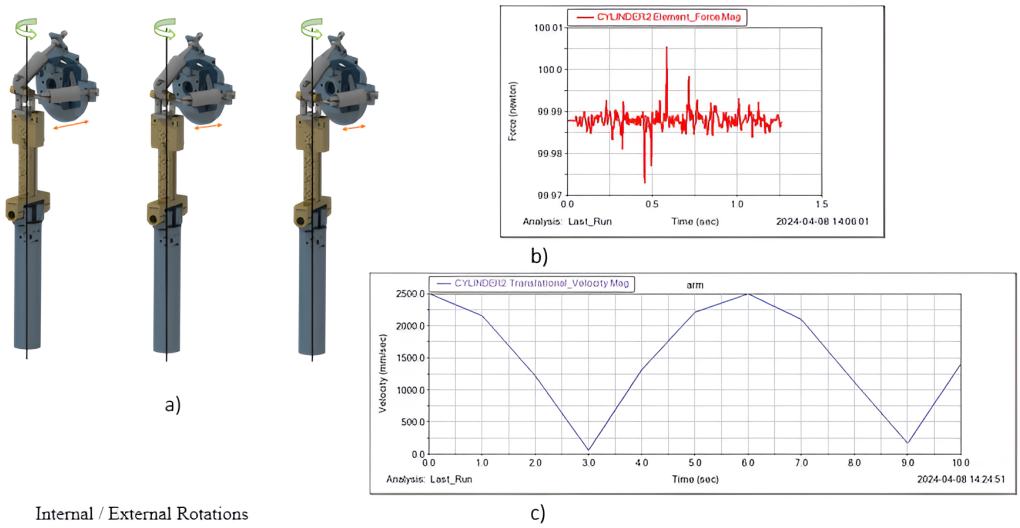

Figure 9. The figure presents the analysis of the shoulder's internal/external rotation. **(a)** illustrates the rotational movement of the arm; **(b)** shows the force required from the hydraulic cylinder to achieve this rotation, with a peak force of approximately 100 N; **(c)** confirms the angular speed of the rotation, being consistent with the simulated harmonic motion.

The torque for flexion/extension was additionally evaluated with a 200 N load applied at the end-effector, as illustrated in Figure 10. Assessing the torque under this 200 N load offers important insights into the shoulder joint's capability when subjected to realistic operational stresses. The observed rise in torque highlights the joint's capacity to adjust and produce adequate force to counteract the extra load imposed on the arm during flexion/extension movements.

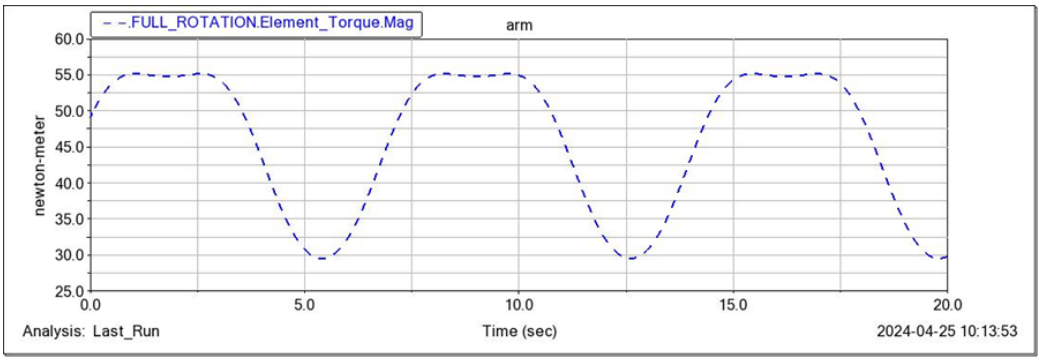

Figure 10. Flexion/Extension torque at 200 N load.

5. Conclusion

This paper introduces a new, hybrid shoulder joint for a hydraulically powered humanoid robot. The design combines serial and parallel parts to give the robot a high range of motion and the ability to carry heavy loads. This approach offers a powerful, compact, and highly dexterous solution for humanoid robots.

The Direct Geometric Model (DGM) of the mechanism was created and an optimized shoulder kinematic configuration was established. The first quantitative verification was the workspace, to expose the ability of the mechanism to move through a large and useful range of motion. The mechanism benchmarked a Workspace Analysis Similarity for Robotic Arms WAS_{RA} measure of 26.13% at the shoulder joint only exceeding by that the ability of state-of-the-art robotic systems like Atlas (17.41%) that has this result for more than one actuated joint at the arm. This shows the efficiency of our proposed hybrid approach towards generating human-like movement at reduced actuation.

Furthermore, no-load and 200 N load condition torque simulations demonstrated the dependability of the mechanism by achieving the highest torque of 68 N·m during flexion/extension movement. This is better than the performance of such state-of-the-art mechanisms in range and reliability while dealing with loads. The mechanism's hydraulic actuators delivered repeatable consistent force outputs of as much as a maximum of 590 N abduction/adduction and 100 N internal/external rotations, showing a strong force development process of the mechanism. One such finding that proves this is that in a study on the RBR-2RRR shoulder joint structure where a parallel hybrid structure could generate high-torque dynamic outputs without compromising range and accuracy of operation [37].

Though the proposed hybrid mechanism shows advantage in terms of workspace and compactness, the inherent trade-offs should be noted. The kinematic complexity of its closed-chain architecture, particularly in the derivation of the inverse geometric model for real-time control, is a major challenge compared to less complicated serial chain robots. The complicated integration of hydraulic elements may also introduce manufacturing and long-term servicing complexity. For instance, the system is more vulnerable to issues like fluid leakage. These limitations, as much as they are possible, are important

considerations for future design updates to balance simplicity and compact high-performance actuation.

Overall, this hybrid mechanism shows strong potential to advance humanoid robotics, especially for tasks that require highly human-like and dexterous movements. Our future work will focus on developing advanced control techniques to ensure the mechanism's motion is smooth, coordinated, and energy-efficient. We will also derive and validate the Inverse Kinematic Model (IKM) for real-time control and perform a comprehensive dynamic analysis to evaluate the mechanism's performance during highly dynamic tasks.

Author's contribution

Conceptualization, A.T.; methodology, W.S.; software, W.S.; validation, H.S. and S.A.; formal analysis, M.S.; investigation, W.S.; resources, W.S.; data curation, W.S.; writing—original draft preparation, W.S.; writing—review and editing, M.S.; visualization, M.S.; supervision, H.S. and S.A.; project administration, S.A. All authors have read and agreed to the published version of the manuscript.

Conflicts of interests

Hang Su holds the position of Associate Editor for *Mechatronics Technology* and has not peer reviewed or made any editorial decisions for this paper.

References

[1] Nelson G, Saunders A, Playter R. The PETMAN and atlas robots at Boston dynamics. In *Humanoid Robotics: A Reference*, 1st ed. Dordrecht: Springer, 2019. pp. 169–186.

[2] Development of a humanoid robot prototype, HRP-5P, capable of heavy labor. 2018. Available: https://www.aist.go.jp/aist_e/list/latest_research/2018/20181116/en20181116.html (accessed on 3 April 2025).

[3] Shigemi S. ASIMO and humanoid robot research at Honda. In *Humanoid Robotics: A Reference*, 1st ed. Dordrecht: Springer, 2019. pp. 55–90.

[4] Figure AI, Inc. Figure 01 humanoid robot. 2024. Available: https://www.figure.ai/figure-01 (accessed on 17 September 2025).

[5] Lambert F. Tesla unveils Optimus Gen 2: its next generation humanoid robot. 2023. Available: https://electrek.co/2023/12/12/tesla-unveils-optimus-gen-2-next-generation-humanoid-robot/ (accessed on 1 June 2025).

[6] Stasse O, Flayols T, Budhiraja R, Giraud-Esclasse K, Carpentier J, *et al*. TALOS: a new humanoid research platform targeted for industrial applications. In *2017 IEEE-RAS 17th International Conference on Humanoid Robotics (Humanoids)*, Birmingham, UK, November 15–17, 2017, pp. 689–695.

[7] Unitree H1-2. 2025. Available: https://support.unitree.com/home/en/H1_developer/About_H1-2 (accessed on 23 September 2025).

[8] Yoshida E. Robots that look like humans: a brief look into humanoid robotics. *Metode Sci. Stud. J.* 2019, 9:143–151.

[9] Okada M, Nakamura Y. Development of a cybernetic shoulder-a 3-DOF mechanism that imitates biological shoulder motion. *IEEE Trans. Rob.* 2005, 21(3):438–444.

[10] Parmiggiani A, Maggiali M, Natale L, Nori F, Schmitz A, *et al*. The design of the iCub humanoid robot. *Int. J. Human. Robot.* 2012, 9(4):1250027.

[11] Albu-Schäffer A, Haddadin S, Ott C, Stemmer A, Wimböck T, *et al.* The DLR lightweight robot: design and control concepts for robots in human environments. *Ind. Robot* 2007, 34(5):376–385.

[12] Herron CW, Fuge AJ, Beiter BC, Fuge ZJ, Tremaroli NJ, *et al*. PANDORA: the open-source, structurally elastic humanoid robot. *arXiv* 2024, arXiv:2407.18558.

[13] Folgheraiter M, Aubakir B. Design and modeling of a lightweight and low power consumption full-scale biped robot. *Int. J. Human. Robot.* 2018, 15(5):1850022.

[14] Asswad ME, AlFayad S, Khalil K. Optimization of HYDROïD robot foot. 2025. Available: https://1library.net/document/y491eekz-optimization-of-hydro-id-robot-foot.html (accessed on 9 June 2025).

[15] Chen F, Carbonari L, Canali C, D'Imperio M, Cannella F. Design of a novel dexterous robotic gripper for in-hand twisting and positioning within assembly automation. *Assem. Autom.* 2015, 35(3):259–268.

[16] Kovacs G, Lochmatter P, Wissler M. An arm wrestling robot driven by dielectric elastomer actuators. *Smart Mater. Struct.* 2007, 16(2):S306.

[17] Briot S, Bonev I. Are parallel robots more accurate than serial robots? *Trans. Can. Soc. Mech. Eng.* 2007, 31(4):445–455.

[18] Harib KH, Moustafa KA, Ullah AS, Zenieh S. Parallel, serial and hybrid machine tools and robotics structures: comparative study on optimum kinematic designs. In *Serial and Parallel Robot Manipulators—Kinematics, Dynamics, Control and Optimization*, 1st ed. Rijeka: InTech, 2012.

[19] Delgado P, Alekhya S, Majidirad A, Hakansson NA, Desai J, *et al.* Shoulder kinematics assessment towards exoskeleton development. *Appl. Sci.* 2020, 10(18):6336.

[20] Otani T, Hashimoto K, Miyamae S, Ueta H, Natsuhara A, *et al*. Upper-body control and mechanism of humanoids to compensate for angular momentum in the yaw direction based on human running. *Appl. Sci.* 2018, 8(1):44.

[21] Klopčar N, Lenarčič J. Kinematic model for determination of human arm reachable workspace. *Meccanica* 2005, 40(2):203–219.

[22] Chandler RF, Clauser CE, Mcconville JT, Reynolds HM, Young JW. Investigation of inertial properties of the human body. 1975. Available: https://apps.dtic.mil/sti/tr/pdf/ADA016485.pdf (accessed on 14 September 2025).

[23] Perera J, Visinsky M, Laske E, Artemiadis P, Heer E, *et al.* Robotic systems safety. In *Safety Design for Space Systems*, 2nd ed. Oxford: Butterworth-Heinemann, 2023. pp. 1033–1082.

[24] Cao Y, Lu K, Li X, Zang Y. Accurate numerical methods for computing 2D and 3D robot workspace. *Int. J. Adv. Rob. Syst.* 2011, 8:76.

[25] Khatib O, Demircan E, Sapio VD, Sentis L, Besier T, *et al.* Robotics-based synthesis of human motion. *J. Physiol Paris* 2009, 103(3–5):211–219.

[26] Leal-Naranjo JA, Ceccarelli M, Torres-San Miguel CR. Mechanical design of a prosthetic human

arm and its dynamic simulation. In *25th Conference on Robotics in Alpe-Adria-Danube Region (RAAD 2016)*, Belgrade, Serbia, June 30–July 2, 2017, pp. 482–490.

[27] Wang Y, Li W, Togo S, Yokoi H, Jiang Y. Survey on main drive methods used in humanoid robotic upper limbs. *Cyborg. Bionic. Syst.* 2021, 2021:9817487.

[28] Pott A. Cable-driven parallel robots: theory and application. In *Springer Tracts in Advanced Robotics*, 1st ed. Cham: Springer International Publishing, 2018.

[29] Mason MT. Mechanics of robotic manipulation. In *The MIT Press*, 1st ed. Cambridge: The MIT Press, 2001.

[30] Lung-Wen T. Mechanism design: enumeration of kinematic structures according to function. *J. Mech. Des.* 2000, 122(4):583.

[31] Tayba A. Improvement of the upper body of HYDROïD robot for bi-manual tasks and manipulation. Doctoral Thesis, Université Paris Saclay (COmUE), 2017.

[32] Alfayad S, Ouezdou FB, Namoun F, Bruneau O, Henaff P. Three DOF hybrid mechanism for humanoid robotic application: modeling, design and realization. In *2009 IEEE/RSJ International Conference on Intelligent Robots and Systems*, St. Louis, USA, October 11–15, 2009, pp. 4955–4961.

[33] Wang W, Wang P, Zhao Y, Zhu Y, Zhao J. Kinematics and workspace analysis of a robotic arm for medical delivery robots. In *E3S Web of Conferences*, Xiamen, China, April 9–11, 2021, p. 01067.

[34] Sanguino TM, Márquez JA. Simulation tool for teaching and learning 3d kinematics workspaces of serial robotic arms with up to 5-dof. *Comput. Appl. Eng. Educ.* 2012, 20:750–761.

[35] Luo J, Wen Q, He J, Ye B. Workspace analysis of 7-dof humanoid robotic arm. In *International Conference on Intelligent Systems Research and Mechatronics Engineering (ISRME 2015)*, Zhengzhou, China, April 11–13, 2015, pp. 48–51.

[36] Sinha AK, Thalmann NM, Cai Y. Measuring anthropomorphism of a new humanoid hand-arm system. *Int. J. Social Rob.* 2023, 15:1341–1363.

[37] Shi S, Wang F, Zhou Y. Configuration and parameter optimization design of a novel rbr-2rrr spherical hybrid bionic shoulder joint. *Machines* 2024, 12:683.